SEMARAK ILMU PUBLISHING

Journal of Advanced Research in Numerical Heat Transfer

Journal homepage:
https://semarakilmu.com.my/journals/index.php/arnht/index
ISSN: 2735-0142

Comparison Study Between Galerkin Finite Element Method and Finite Volume Method for Diffusion Problem

Wah Yen Tey[1,2*], Yutaka Asako[1], Keng Yinn Wong[3]

[1] Malaysia-Japan International Institute of Technology, University Teknologi Malaysia, Kuala Lumpur, Malaysia
[2] Department of Mechanical Engineering, Faculty of Engineering, Technology, and Built Environment, UCSI University, Kuala Lumpur, Malaysia
[3] Faculty of Mechanical Engineering, Universiti Teknologi Malaysia, Skudai, Johor, Malaysia

ARTICLE INFO

Article history:
Received 30 September 2023
Received in revised form 19 October 2023
Accepted 21 November 2023
Available online 31 December 2023

Keywords:
Galerkin finite element method; Finite volume method; Steady diffusion; Transient diffusion

ABSTRACT

The finite element method (FEM) is a robust and widely applied numerical scheme in the simulation of engineering problems, especially in structural mechanics. However, FEM is not as popular as the finite volume method (FVM) in Computational Fluid Dynamics (CFD), possibly due to its complicated numerical procedures. Indeed, FEM possesses tremendous advantages compared with FVM, particularly in dealing with complex geometry and rendering attractive flexibility to modify the interpolation functions. It is well-known that FEM and FVM differ in mathematical formulation, yet there is a lack of practical comparison between them. Therefore, the paper aims to develop a Galerkin FEM (GFEM) model, investigate its strengths and weaknesses compared with FVM, and discuss the conciliation between FEM and FVM. Our case study focuses on a two-dimensional diffusion problem comprising steady and transient cases, with and without heat generation. Our investigation revealed that GFEM does not possess conservative properties, which might yield spurious heat flux, leading to a 2 – 4% overestimation of the temperature field, depending on the amount of heat generation. Moreover, GFEM incurs approximately 34% higher computational time than FVM. However, FVM can be perceived as a special form of GFEM, and their relations were discussed.

1. Introduction

The finite element method (FEM) is a numerical scheme to solve boundary value problems via integration over the weighted variational form of governing equations [1]. Since its introduction, FEM has been mainly applied in the analysis of structural engineering, such as welding analysis [2], machining of composite materials [3], buckling analysis [4], mechanical vibration [5,6], design of biomedical structures [7,8], and fatigue prediction of structures [9,10]. FEM has been well developed in solving structural mechanics, and much commercial software such as COMSOL® and SolidWorks® are constructed thereunder.

* *Corresponding author.*
E-mail address: Wahyen.Tey@gmail.com or teywy@ucsiuniversity.edu.my (Wah Yen Tey)

https://doi.org/10.37934/arnht.15.1.2442

However, in thermofluidic simulation, FEM is not as popular as the finite volume method (FVM) due to its complexity and high computational cost compared with FVM. In FVM, the nodal fields can be correlated via the integration over the surface of the control volume; thus, its stiffness matrix formulation is relatively straightforward. FVM solution is formulated based on the analysis of fluxes across boundaries, while FEM forms the stiffness matrix by interpolating the nodes around a local boundary. Notably, FVM emphasises the conservativeness properties of transport phenomena [11]. At the same time, FEM focuses more on approximating suitable local guess functions that can fulfil governing equations and boundary conditions. Perhaps, FVM is an indigenous numerical solution for Computational Fluid Dynamics (CFD), and as such many essential techniques in CFD, such as SIMPLE algorithms [12–14] and immersed boundary methods [15–17], are designed based on FVM.

Despite these limitations, FEM is more robust in dealing with complex geometry. Its elementary integration on the local boundary would relieve the meshing constraints when the geometry of the problem domain is arbitrary. Moreover, FEM is the rudiments of meshfree techniques developed to solve thermofluidic problems with moving interfaces. Examples of meshfree methods are the element-free Galerkin method [18–22], point interpolation meshfree method [23], and meshfree local Petrov-Galerkin method [24], to name a few. These meshfree methods could be an alternative to immersed boundary methods. It is worth transplanting the formulation of FEM into CFD; thus, a more detailed investigation between FVM and FEM is required.

Most of the previous works comparing FEM and FVM focused only on the theoretical explanations, such as in the work of Soln [25] and Vanselow [26]. A general comparison can be seen too in the work of Ahmad *et al.,* [27] and Dong *et al.,* [28], who simulated macrosegregation and electrical impedance tomography, respectively. Jeong and Seong [29] carried out a comparison between FEM and FVM commercial software. However, there needs to be a detailed comparison by numerical examples, especially in the heat transfer problem.

Simulation on pure diffusion can be perceived as CFD's most straightforward platform for numerical testing. The one-dimensional heat transfer problem has been solved using FEM by Wang and Mai [30] and Dhawan and Kumar [31], and it is simple and straightforward. Although FEM and FVM will not reveal any difference in solving the one-dimensional problem, computational complexity would significantly increase when the problem domain is two-dimensional.

There is a void in practical comparison and relations between FEM and FVM, although their difference in the mathematical formulation has been well explained [32]. Therefore, the paper aims to: (1) develop a lucid formulation of the Galerkin finite element method (GFEM) for the convenience of future development, (2) discuss the differences between FEM and FVM, and (3) investigate the relations and conciliations between FEM and FVM. In our study, both steady and transient diffusion, with and without heat generation, are included. The work can provide a detailed reference to assess the differences and reconciliations between these two widely applied discretisation techniques.

2. Numerical Formulation

The governing equation for the unsteady diffusion problem can be expressed in Eq. (1).

$$\rho C_P \frac{\partial T}{\partial t} = k\left(\frac{\partial^2 T}{\partial x^2} + \frac{\partial^2 T}{\partial y^2}\right) + Q \tag{1}$$

where T = temperature (K), C_P = specific heat (J/kg.K), ρ = density (kg/m^3), k = thermal conductivity (W/m.K) and Q = heat generation (W/m^3). The Dirichlet boundary condition is assumed around the problem domain, which is a 1 m × 1 m square plate, as shown in Figure 1.

T_W, T_S, T_E, and T_N represent the boundary temperature at the West, South, East, and North boundary, respectively. In this study, the values of constants applied are C_P = 910 J/kg.K, ρ = 2710 kg/m^3, k = 205 W/m.K and Q = 400 kW/m^3. Only the Dirichlet boundary condition is assumed. The temperatures at the edges at T_W, T_S, T_E and T_N are set as 300K, 500K, 700K and 1000K, respectively. For the transient case, the initial temperature is assumed as 283 K. To ensure the consistency of comparison between both methods; we avoided the interference of mesh structure on the results by applying a structured Cartesian mesh with a similar mesh size for both GFEM and FVM.

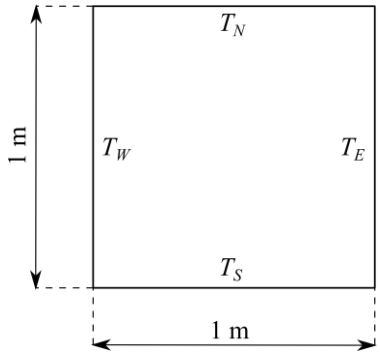

Fig. 1. The problem domain of the 2D diffusion problem

2.1 Galerkin Finite Element Method

In GFEM, interpolation function N is included in the governing equation before integration occurs. Eq. (1) is integrated to form Eq. (2):

$$\int_{\Omega} w\left[k\left(\frac{\partial^2 T}{\partial x^2}+\frac{\partial^2 T}{\partial y^2}\right)+Q-\rho C_P\frac{\partial T}{\partial t}\right]d\Omega=0 \tag{2}$$

where Ω is the problem domain, while w is the weight function. In the GFEM, the weight function is equivalent to the interpolation function. Using quadratic interpolation techniques as illustrated in Figure 2, the interpolation functions can be assumed as N_1 = (1–x)(1–y)/4, N_2 = (1+x)(1–y)/4, N_3 = (1+x)(1+y)/4 and N_4 = (1–x)(1+y)/4.

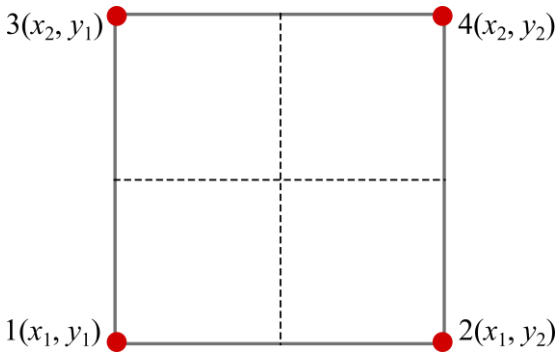

Fig. 2. Quadratic interpolation scheme for element in GFEM

Integrating Eq. (2) by part will form:

$$\int_{\Omega}\left(NQ\right)d\Omega-\int_{\Omega}\left(N\rho C_P\frac{\partial T}{\partial t}\right)d\Omega-\int_{\Omega}\left(k\frac{\partial N}{\partial x}\frac{\partial T}{\partial x}\right)d\Omega-\int_{\Omega}\left(k\frac{\partial N}{\partial y}\frac{\partial T}{\partial y}\right)d\Omega$$
$$+\int_{\Gamma}\left(Nk\frac{\partial T}{\partial x}\right)d\Gamma+\int_{\Gamma}\left(Nk\frac{\partial T}{\partial y}\right)d\Gamma=0 \tag{3}$$

in which the integrated equation in Eq. (3) signifies the integration over the volume (for three-dimensional cases) or area (two-dimensional cases) of the element. Γ represents the edges of the element. Upon integration over the element domain, the first and second terms in Eq. (3) become Eq. (4) and Eq. (5), respectively.

$$\int_{\Omega}\left(NQ\right)d\Omega=Q\Delta x\Delta y=\left[k^{(e)}{}_{Q}\right] \tag{4}$$

$$\int_{\Omega}\left(N\rho C_P\frac{\partial T}{\partial t}\right)d\Omega=\rho C_P\Delta x\Delta y\left(\int_t\frac{\partial T}{\partial t}dt\right)=\left[k^{(e)}{}_{Tr}\right]\left(\int_t\frac{\partial T}{\partial t}dt\right) \tag{5}$$

Meanwhile, the third and fourth terms in Eq. (3) can be developed using the Galerkin approach to form a local stiffness matrix. In GFEM, the approximated temperature field is:

$$T^h=T_1N_1\left(x,y\right)+T_2N_2\left(x,y\right)+T_3N_3\left(x,y\right)+T_4N_4\left(x,y\right) \tag{6}$$

where T_1, T_2, T_3, and T_4 represents the temperature at location 1, 2, 3, and 4, respectively, as shown in Figure 2. By substituting Eq. (6) into the third and fourth terms in Eq. (3),

$$\int_{\Omega}\left(k\frac{\partial N}{\partial x}\frac{\partial T}{\partial x}\right)d\Omega-\int_{\Omega}\left(k\frac{\partial N}{\partial y}\frac{\partial T}{\partial y}\right)d\Omega=k\int_{y_1}^{y_2}\int_{x_1}^{x_2}\left(\left[\frac{\partial N_i}{\partial x}\right]^T\left[\frac{\partial N_i}{\partial x}\right]+\left[\frac{\partial N_i}{\partial y}\right]^T\left[\frac{\partial N_i}{\partial y}\right]\right)\left\{\mathbf{T}\right\}dxdy \tag{7}$$

taking:

$$\int_{y_1}^{y_2}\int_{x_1}^{x_2}\left(\left[\frac{\partial N_i}{\partial x}\right]^T\left[\frac{\partial N_i}{\partial x}\right]+\left[\frac{\partial N_i}{\partial y}\right]^T\left[\frac{\partial N_i}{\partial y}\right]\right)dxdy=\left[k^{(e)}\right] \tag{8}$$

Then Eq. (7) can be written in a simpler form:

$$\int_{\Omega}\left(\frac{\partial N}{\partial x}\frac{\partial T}{\partial x}\right)d\Omega-\int_{\Omega}\left(\frac{\partial N}{\partial y}\frac{\partial T}{\partial y}\right)d\Omega=\left[k^{(e)}\right]\left\{\mathbf{T}\right\} \tag{9}$$

Upon analytical integration on Eq. (7) based on quadratic interpolation techniques, a local stiffness matrix can be formed as in Eq. (10). The principle of the derivation of GFEM formulation can be found in Ref. [33].

$$\left[k^{(e)}\right]=\begin{bmatrix} k_{11} & k_{12} & k_{13} & k_{14} \\ k_{21} & k_{22} & k_{23} & k_{24} \\ k_{31} & k_{32} & k_{33} & k_{34} \\ k_{41} & k_{42} & k_{43} & k_{44} \end{bmatrix}=\begin{bmatrix} 2/3 & -1/6 & -1/3 & -1/6 \\ -1/6 & 2/3 & -1/6 & -1/3 \\ -1/3 & -1/6 & 2/3 & -1/6 \\ -1/6 & -1/3 & -1/6 & 2/3 \end{bmatrix} \tag{10}$$

The local stiffness matrix in Eq. (10) must be expanded to form a global stiffness matrix. By taking the number of nodes in the problem domain as 3 × 3 as an example, a simple, symmetry global stiffness matrix can be formed as in Eq. (11). The Dirichlet boundary condition has been included in the equation.

$$\begin{bmatrix} 8/3 & -2/6 & 0 & -2/3 & -1/6 & 0 & 0 & 0 & 0 \\ -2/6 & 8/3 & -2/6 & -1/6 & -2/3 & -1/6 & 0 & 0 & 0 \\ 0 & -2/6 & 8/3 & 0 & -1/6 & -2/3 & 0 & 0 & 0 \\ -2/3 & -1/6 & 0 & 8/3 & -2/6 & 0 & -2/3 & -1/6 & 0 \\ -1/6 & -2/3 & -1/6 & -2/6 & 8/3 & -2/6 & -1/6 & -2/3 & -1/6 \\ 0 & -1/6 & -2/3 & 0 & -2/6 & 8/3 & 0 & -1/6 & -2/3 \\ 0 & 0 & 0 & -2/3 & -1/6 & 0 & 8/3 & -2/6 & 0 \\ 0 & 0 & 0 & -1/6 & -2/3 & -1/6 & -2/6 & 8/3 & -2/6 \\ 0 & 0 & 0 & 0 & -1/6 & -2/3 & 0 & -2/6 & 8/3 \end{bmatrix}\begin{bmatrix} T_{1,1} \\ T_{1,2} \\ T_{1,3} \\ T_{2,1} \\ T_{2,2} \\ T_{2,3} \\ T_{3,1} \\ T_{3,2} \\ T_{3,3} \end{bmatrix}=\begin{bmatrix} (1/2)T_W \\ 0 \\ (1/2)T_E \\ (2/3)T_W \\ 0 \\ (2/3)T_E \\ (1/2)T_W \\ 0 \\ (1/2)T_E \end{bmatrix}+\begin{bmatrix} (2/3+1/6)T_S \\ (2/3+1/3)T_S \\ (2/3+1/6)T_S \\ 0 \\ 0 \\ 0 \\ (2/3+1/6)T_N \\ (2/3+1/3)T_N \\ (2/3+1/6)T_N \end{bmatrix} \tag{11}$$

Eq. (11) must be further expanded according to the prescribed number of nodes. Now by applying Green's Theorem to integrate the last two terms of Eq. (3), Eq. (12) can be formed.

$$\int_\Gamma \left(Nk\frac{\partial T}{\partial x}\right)d\Gamma+\int_\Gamma \left(Nk\frac{\partial T}{\partial y}\right)d\Gamma=k\oint_S N_i\left(q_x\cdot\overrightarrow{n_x}+q_y\cdot\overrightarrow{n_y}\right)ds \tag{12}$$

In the current study, Green's integrals of Eq. (12) can be eliminated since zero heat flux is assumed throughout the domain. Combining Eqs. (4), (5) and (9) into Eq. (3), Eq. (13) can be formed.

$$\left[k^{(e)}{}_Q\right]+\left[k^{(e)}{}_{Tr}\right]\left(\int_t \frac{\partial T}{\partial t}dt\right)+k\left[k^{(e)}\right]\{\mathbf{T}\}=0 \tag{13}$$

Eq. (14) can be yielded for computation of transient conduction problem by taking the time integral via the implicit method,

$$\therefore\left(\left[k^{(e)}{}_{Tr}\right]^D+\left[k^e\right]\right)\{\mathbf{T}^{n+1}\}=\frac{1}{k}\left[k^{(e)}{}_Q\right]+\left[k^{(e)}{}_{Tr}\right]^V\{\mathbf{T}^n\} \tag{14}$$

The superscripts *D* and *V* represent diagonal and vertical matrices, respectively. If the conduction is steady, Eq. (14) is simplified as in Eq. (15).

$$\left[k^{(e)}{}_Q\right]+k\left[k^{(e)}\right]\{\mathbf{T}\}=0 \tag{15}$$

For cases in which there is no heat generation, $Q = 0$.

2.2 Finite Volume Method

Instead of integrating over the problem domain by incorporating the interpolation function of nodes as in GFEM, FVM directly integrates the conservation equation by considering the heat flux across the boundary of the domain. The field variables computed via FVM and GFEM are in the middle and edges of the domain boundary, respectively.

In this paper, the time marching method used is the implicit method. By taking a regular grid size over *x*- and *y*- components, the discretised Eq. (1) via FVM is illustrated as in Eq. (16).

$$-\frac{\rho C_P \Delta x^2}{k\Delta t} T_{i,j}{}^{n} - \frac{Q\Delta x^2}{k} = T_{i-1,j}{}^{n+1} + T_{i+1,j}{}^{n+1} - \left(4 + \frac{\rho C_P \Delta x^2}{k\Delta t}\right) T_{i,j}{}^{n+1} + T_{i,j-1}{}^{n+1} + T_{i,j+1}{}^{n+1} \tag{16}$$

Eq. (16) is transformed into a matrix form to be solved iteratively. Since the detailed formulation of FVM has been widely discussed, such as in the work of Versteeg and Malalasekara [34] and Kajishima and Taira [35], the procedure of matrix formation via FVM will not be elaborated further here.

Perhaps, Eq. (16) can be obtained by the Finite Difference Method (FDM) as well because at a uniform structured grid, both FVM and FDM can be simplified to form a similar equation. However, the FDM is formulated by Taylor series expansion, which differs from the integration over the control volume surface as applied in the FVM. Therefore, although FVM and FDM would lead to a similar equation as in Eq. (16), they are similar but not identical.

Meanwhile, Eq. (16) can be for steady-state diffusion simplified to form Eq. (17).

$$\frac{k}{\Delta x^2}\left(T_{i-1,j}{}^{n+1} + T_{i+1,j}{}^{n+1} - 4T_{i,j}{}^{n+1} + T_{i,j-1}{}^{n+1} + T_{i,j+1}{}^{n+1}\right) = -Q \tag{17}$$

Similarly, for a case in which there is no heat generation, $Q = 0$.

3. Results and Discussion

3.1 Steady-state Heat Conduction

As discussed in the last section, solvers for both GFEM and FVM were developed using MATLAB. The number of nodes applied is 15 × 15, while the grid size is uniform across all the domains, as manifested in Figure 3. For validation purposes, a more straightforward case is applied here. We take T_W, T_S, T_E, and Q are zero while T_N = 1000 K. The analytical solution for the validation case is:

$$T(x,y) = \sum_{n=1}^{\infty} A_n \sin(n\pi x)\sinh(n\pi y) \tag{18}$$

where

$$A_n = \frac{2000}{\sinh(n\pi)}\left(\frac{1-\cos(n\pi)}{n\pi}\right) \tag{19}$$

By taking the temperature along the middle of the *x*-axis, the comparison between the analytical solution, GFEM solution and FVM solution can be shown in Figure 4. Although the GFEM solution is slightly overpredicting the temperature field, its temperature distribution follows the trendline of the analytical solution, in general. Anyhow, FVM has higher accuracy compared with GFEM [36]. The coefficient of the multiple determination (R^2) plot in Figure 5 further proved that FVM could predict the temperature field slightly better than GFEM. The curve's derivative in Figure 5 for GFEM and FVM solution is about 1.0115 and 0.1069, respectively. The lower the curve's derivative, the more accurate the result is. The root means square error (RMSE) for the solution using GFEM and FVM is 48.6076 and 4.4496, respectively. This phenomenon implies that the GFEM solution would give a higher and over-estimated temperature field than the actual solution compared with FVM.

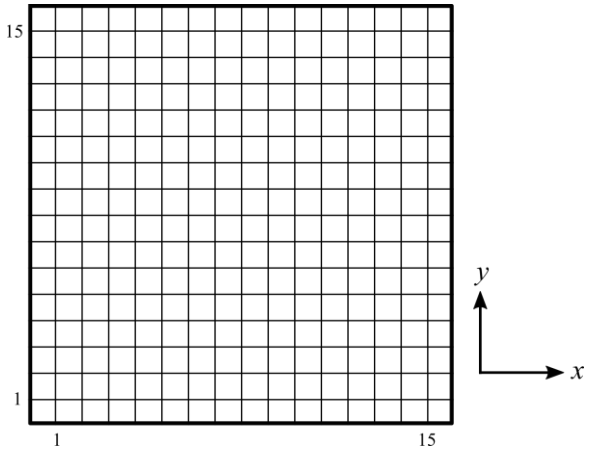

Fig. 3. Uniform meshing for the problem domain with 15 × 15 number of nodes

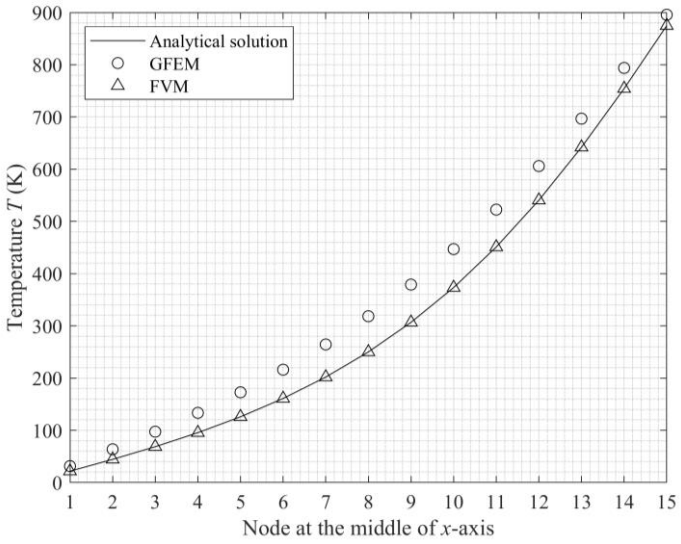

Fig. 4. Comparison between analytical solution, GFEM and FVM for validation case

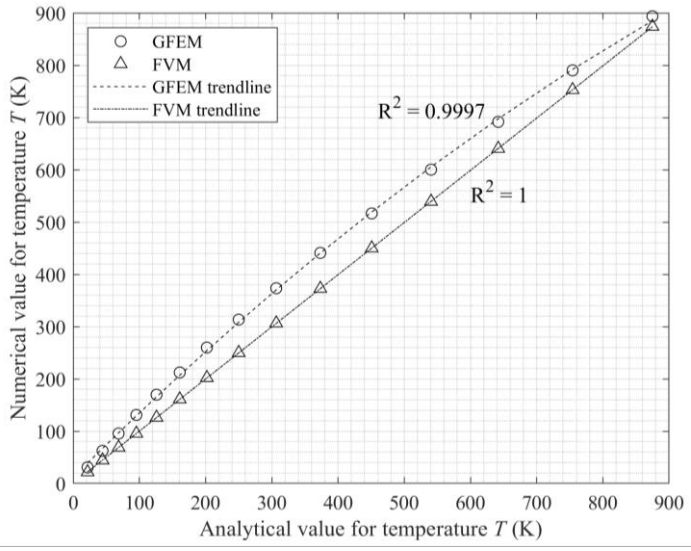

Fig. 5. Coefficient of multiple determination (R^2) plot between analytical solution, GFEM, and FVM

The simulation is expanded with non-zero values for T_W, T_S, T_E, and T_N, as the last section prescribes. The temperature distribution for steady-state conduction, with and without heat generation, has been illustrated in Figure 6. It can be observed that the temperature field predicted by GFEM would have higher value, which is in line with the trendline as shown in Figure 4. The over-prediction of GFEM becomes more apparent when there is heat generation, and this phenomenon can be observed by comparing Figure 6(c) and Figure 6(d).

Upon further scrutiny of the heat fluxes across the boundary (see Eq. 19), based on the temperature computed by GFEM, it can be found that there is a spurious heat flux across the problem domain. By taking steady conduction as an example, the results computed by FVM are almost free from spurious heat flux, while the field variable computed from GFEM is susceptible to spurious heat flux. These residuals of the GFEM results could be because GFEM formulation cannot ensure the conservativeness of heat flux. The erroneous heat flux of GFEM can be demonstrated in Figure 7.

$$\text{Heat flux} = k\oint_S N_i \left(q_x \cdot \overrightarrow{n_x} + q_y \cdot \overrightarrow{n_y}\right) ds = k\oint_S \left(N_i \left.\frac{\partial T}{\partial x}\right|_{x_1}^{x_2} + N_i \left.\frac{\partial T}{\partial y}\right|_{y_1}^{y_2} \right) ds \tag{20}$$

However, FVM may suffer spurious heat flux if there is heat generation, yet it is much lower than GFEM. The spurious heat flux produced by FVM is also more consistent, as shown in Figure 7(d). The spurious heat flux suffered by GFEM is more severe near the corners and boundaries. We also further computed the average spurious heat flux for both methods when heat generation ranges from 0 kW/m^3 to 700 kW/m^3, as illustrated in Figure 8. The magnitude of spurious heat flux increases proportionally with the amount of heat generation. It shows that GFEM generates more spurious heat flux as heat generation increases. Perhaps, GFEM is having approximately 2% more spurious heat flux than FVM.

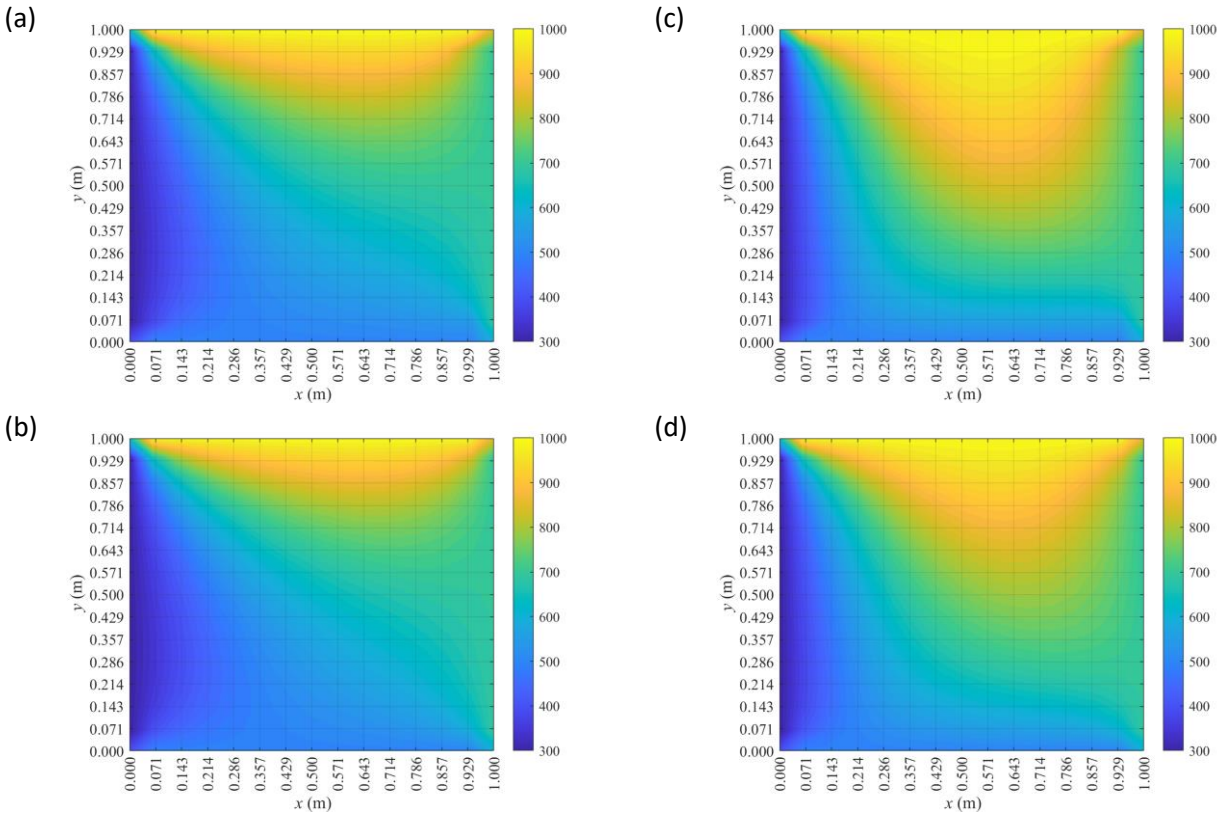

Fig. 6. Temperature distribution on the problem domain without heat generation when: (a) GFEM and (b) FVM are applied; with heat generation (400 kW/m^3) when (c) GFEM and (d) FVM are applied

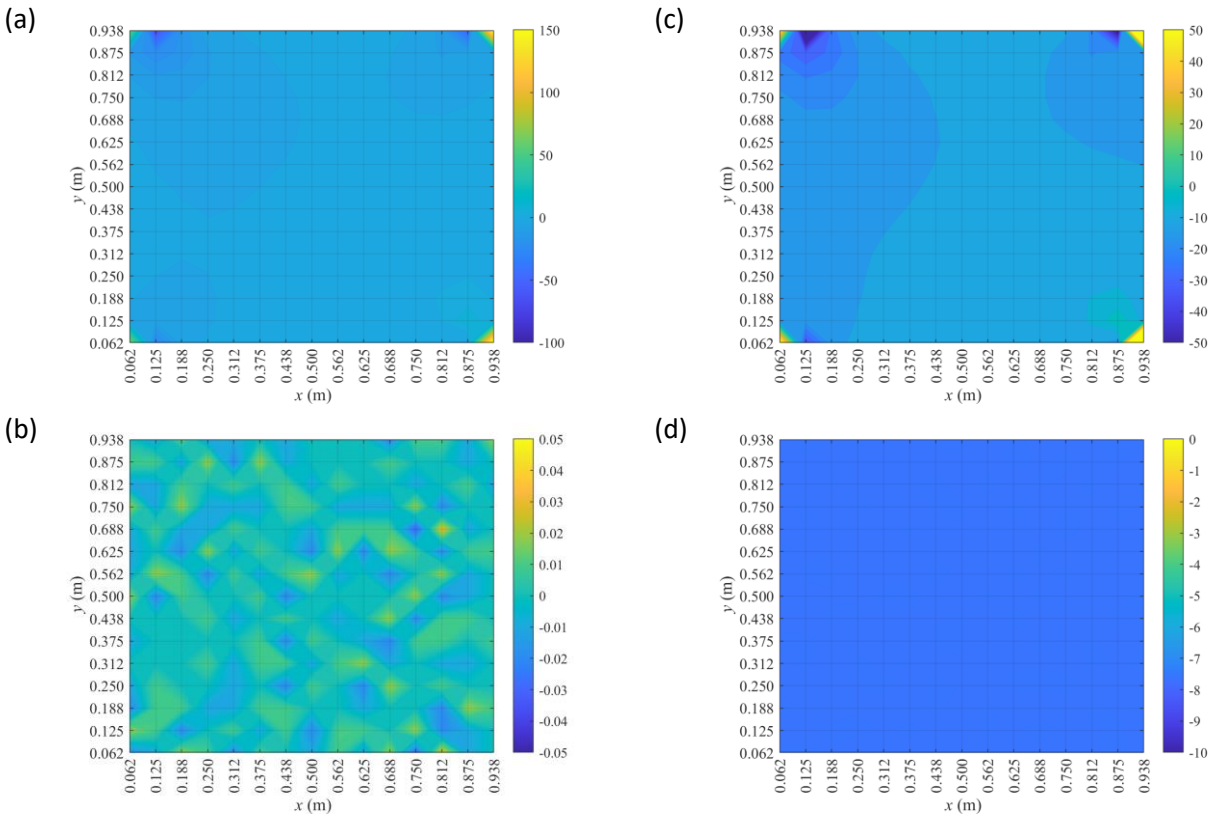

Fig. 7. Spurious heat flux (W/m^2) across the problem domain without heat generation when: (a) GFEM and (b) FVM are applied; with heat generation when (c) GFEM and (d) FVM are applied

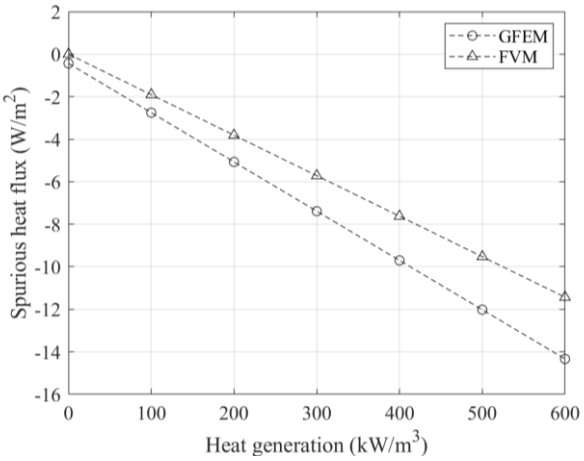

Fig. 8. Average spurious heat flux (W/m^2) across the problem domain using GFEM and FVM due to different amounts of heat generation (W/m^3)

3.2 Transient Heat Conduction

The simulation results for transient heat conduction without and with heat generation (400 kW/m^3) computed using GFEM and FVM are shown in Figure 9 and Figure 10, respectively. The temperature contours were plotted with consistent contour values and spatial coordinates for possible benchmarking in the future. The change of temperature field is captured at 633 seconds, 1265 seconds, 1898 seconds, and 2531 seconds. The initial temperature is set constant at 283 K for all the cases. In the transient case computation, the Courant number (see Eq. 21) of 0.5 ensures stable time marching.

$$\text{Courant number} = \frac{k\Delta t}{\Delta x} \tag{21}$$

The computed temperature change concerning time using GFEM and FVM is demonstrated in Figure 11. The comparison is made when the heat generation is ignored, from top to bottom, at the middle of the *x*-axis. At the early stage of computation, FVM shows a higher value than GFEM. However, when the solution is close to converge, the GFEM would appear to have a 2 – 4% over-prediction of temperature.

3.3 General Comments for Comparison between GFEM and FVM

In general, GFEM exhibits greater numerical errors and spurious heat flux than FVM. Further examination was made to study the effect of mesh size towards its numerical accuracy and computational cost. The mesh size was increased exponentially from 15 × 15 to 55 × 55. The average error (%) for GFEM remained the same (26%) although the mesh size increased exponentially. The high error of GFEM can be due to its un-conservativeness, which will be discussed in detailed later in this section. Meanwhile average error for FVM decreases as the mesh size increased, as illustrated in Figure 12. Moreover, it can be discovered also that the computational time required by GFEM is about 34% than higher than FVM, in all mesh size tested, as shown in Figure 13.

(a) t = 633 seconds, GFEM

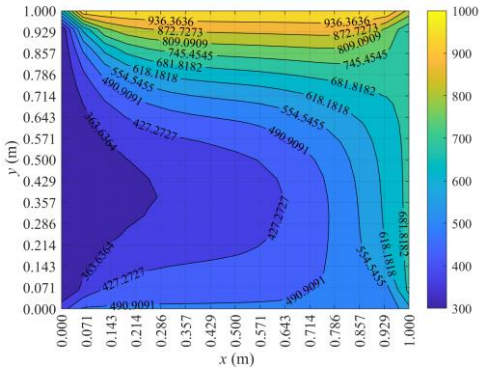

(e) t = 633 seconds, FVM

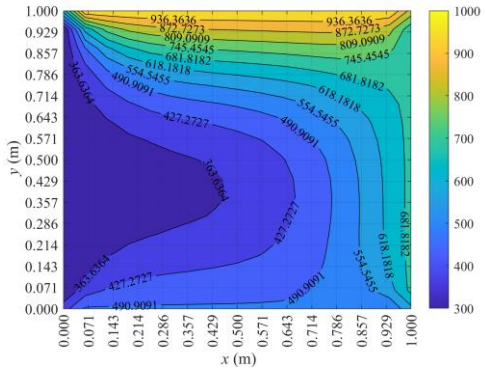

(b) t = 1265 seconds, GFEM

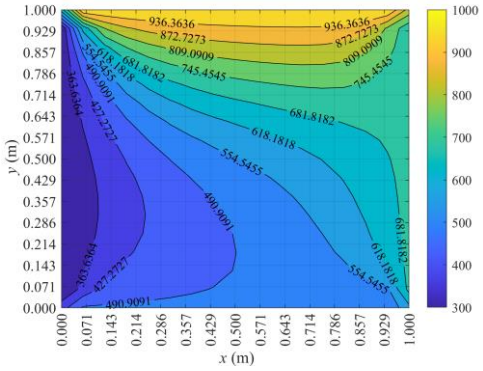

(f) t = 1265 seconds, FVM

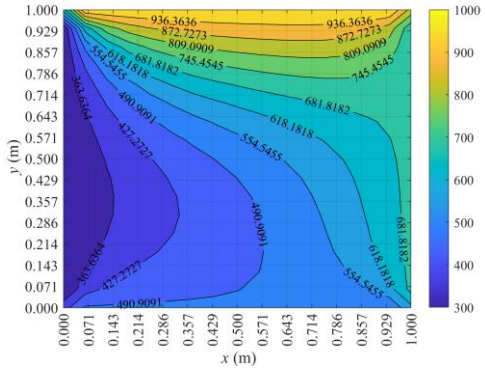

(c) t = 1898 seconds, GFEM

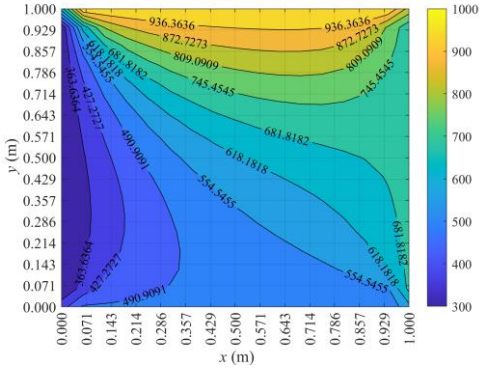

(g) t = 1898 seconds, FVM

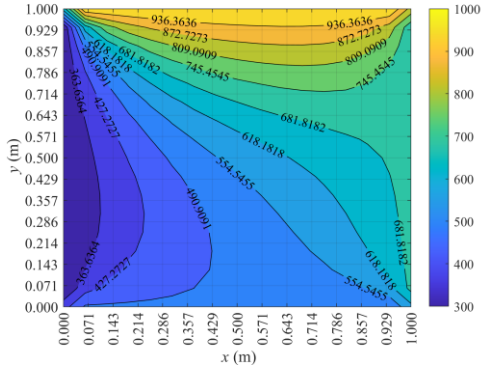

(d) t = 2531 seconds, GFEM

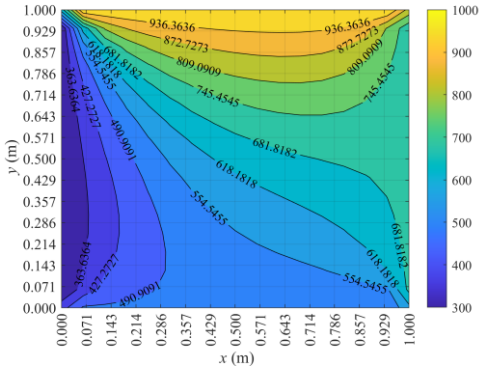

(h) t = 2531 seconds, FVM

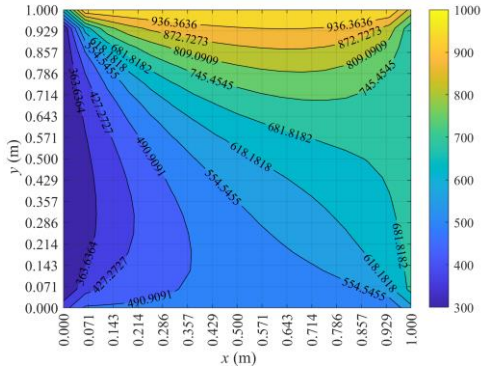

Fig. 9. Temperature field computed using GFEM at (a) 633 seconds, (b) 1265 seconds, (c) 1898 seconds, and (d) 2531 seconds; and FVM at (e) 633 seconds, (f) 1265 seconds, (g) 1898 seconds, and (h) 2531 seconds without heat generation

(a) t = 633 seconds, GFEM

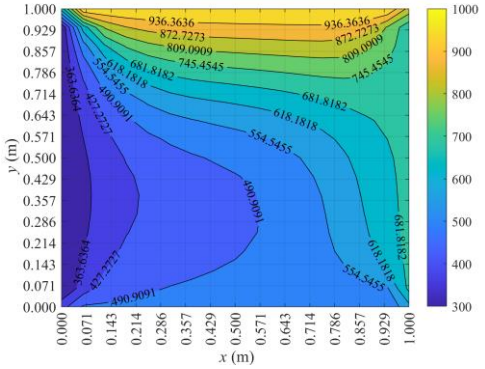

(e) t = 633 seconds, FVM

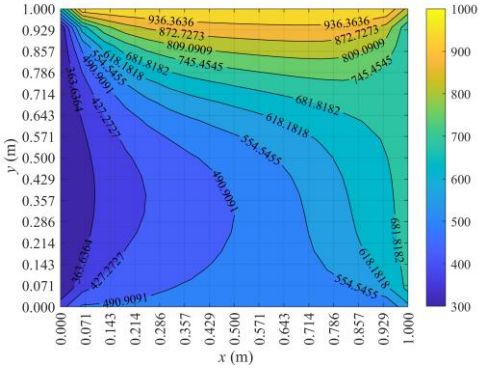

(b) t = 1265 seconds, GFEM

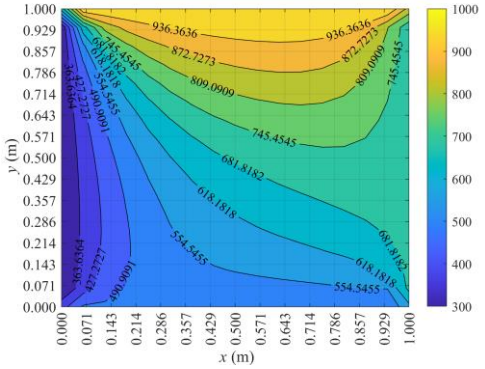

(f) t = 1265 seconds, FVM

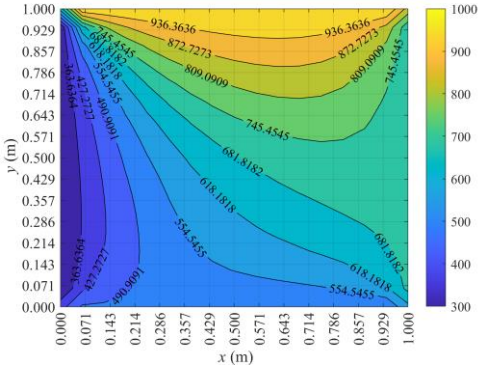

(c) t = 1898 seconds, GFEM

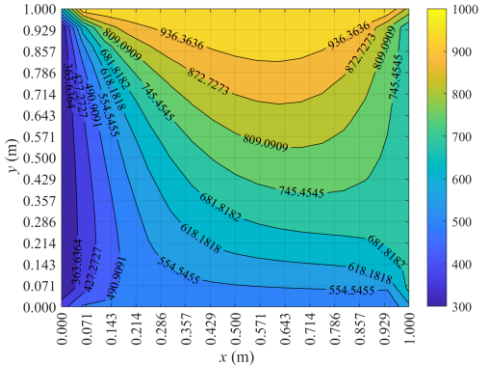

(g) t = 1898 seconds, FVM

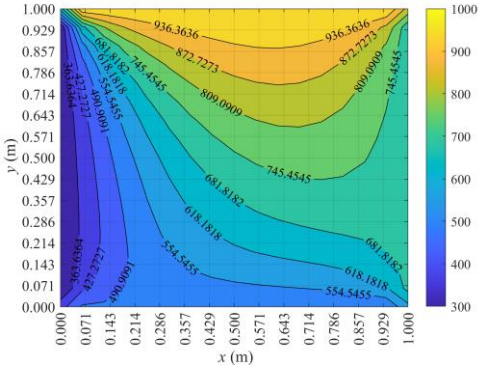

(d) t = 2531 seconds, GFEM

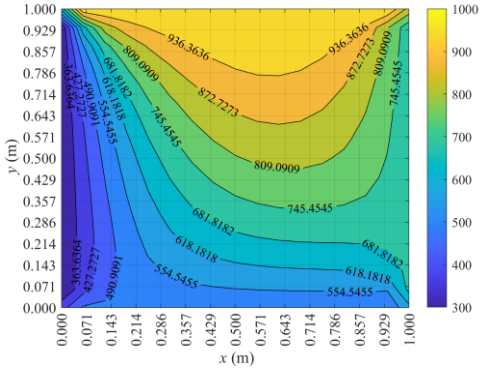

(h) t = 2531 seconds, FVM

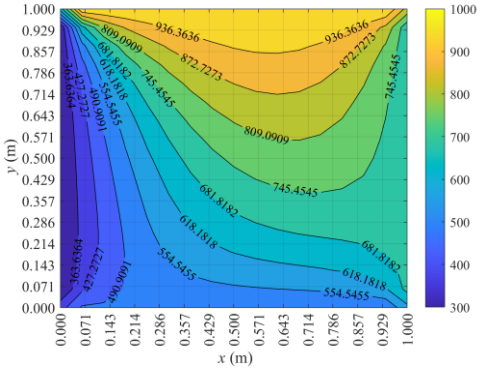

Fig. 10. Temperature field computed using GFEM at (a) 633 seconds, (b) 1265 seconds, (c) 1898 seconds, and (d) 2531 seconds; and FVM at (e) 633 seconds, (f) 1265 seconds, (g) 1898 seconds, and (h) 2531 seconds with heat generation (400 kW/m^3)

(a)

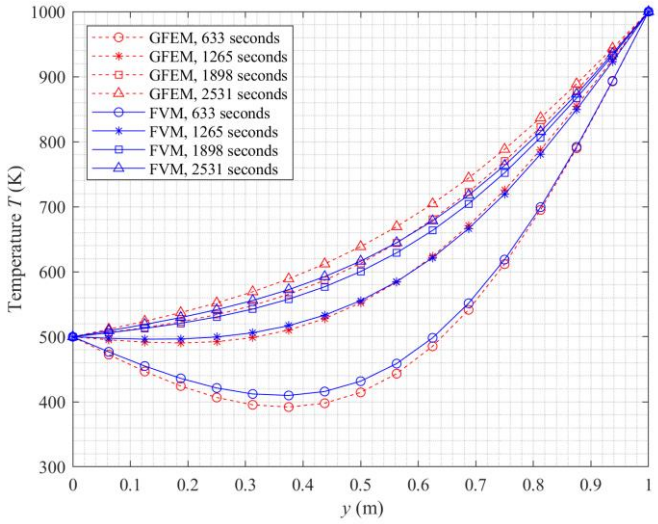

(b)

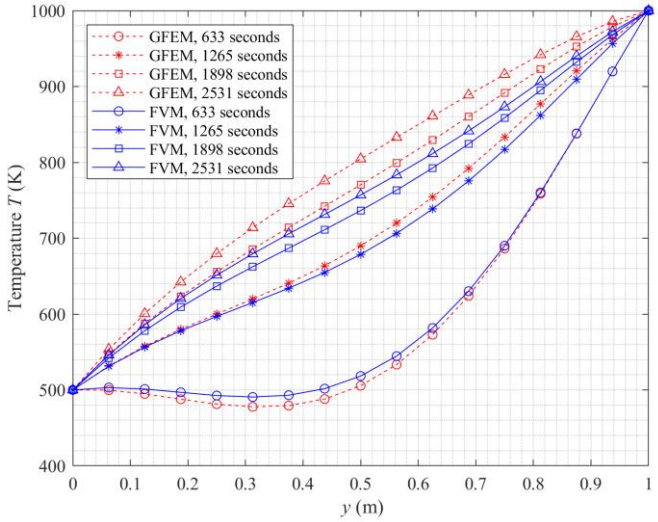

Fig. 11. Comparison of nodal temperature computed using GFEM and FVM at the middle line of the *x*-axis at the different capturing times for the case: (a) without heat generation and (b) with heat generation (400 kW/m^3)

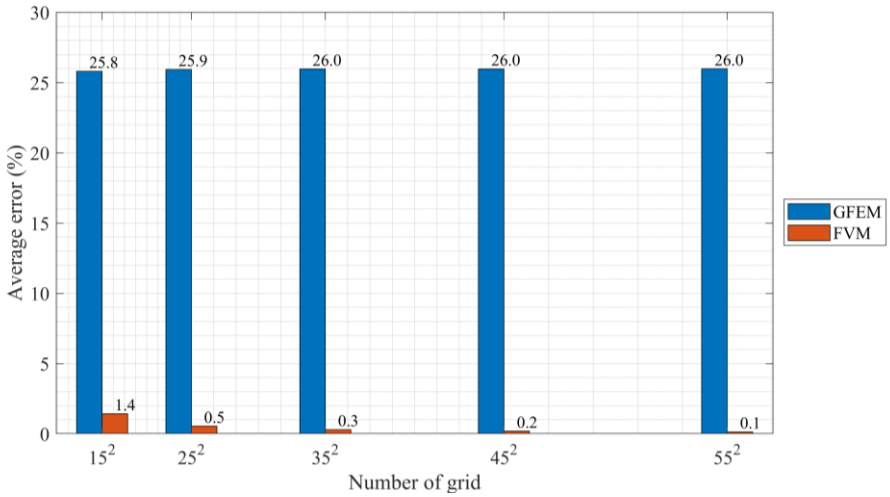

Fig. 12. The relationship between average error (%) with the mesh size of GFEM and FVM

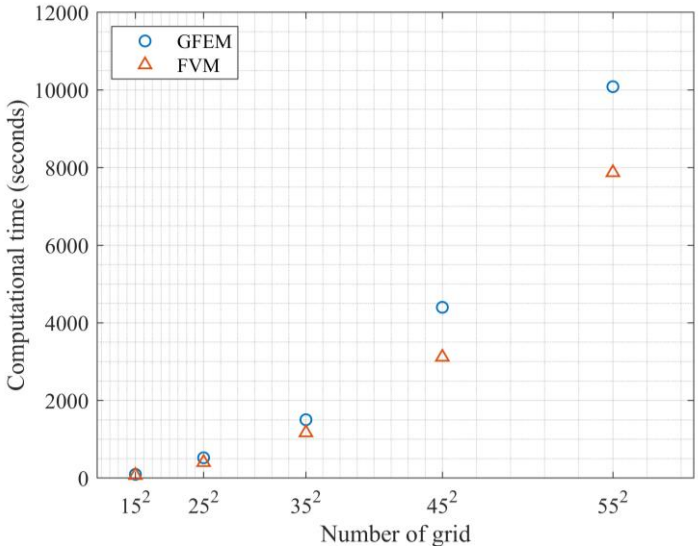

Fig. 13. The computational time required at different the mesh size for GFEM and FVM

3.4 Relations between GFEM and FVM

If we take the weight function *w* in Eq. (2) as unity, i.e., 1, the first derivative of the weight function will produce zero, i.e.,

$$\frac{\partial w}{\partial X}=\frac{\partial N}{\partial X}=\frac{\partial}{\partial X}(1)=0$$

The weak formulation of the governing equation in Eq. (3) can then be simplified to form Eq. (22), perhaps the FVM discretisation technique. Therefore, FVM can also be perceived as a unique form of FEM if *N* = 1 and the heat flux is non-zero. Meanwhile, in FEM, zero heat flux is assumed within the element, and thus Eq. (23) can be formed. The detailed and generic mathematical explanation of the conciliation can be referred to in the work of Wu *et al.,* [37].

$$\int_{\Omega}(NQ)d\Omega-\int_{\Omega}\left(N\rho C_P\frac{\partial T}{\partial t}\right)d\Omega+\int_{\Gamma}\left(Nk\frac{\partial T}{\partial x}\right)d\Gamma+\int_{\Gamma}\left(Nk\frac{\partial T}{\partial y}\right)d\Gamma=0 \tag{22}$$

$$\int_{\Omega}(NQ)d\Omega-\int_{\Omega}\left(N\rho C_P\frac{\partial T}{\partial t}\right)d\Omega-\int_{\Omega}\left(k\frac{\partial N}{\partial x}\frac{\partial T}{\partial x}\right)d\Omega-\int_{\Omega}\left(k\frac{\partial N}{\partial y}\frac{\partial T}{\partial y}\right)d\Omega=0 \tag{23}$$

From Eq. (22) and Eq. (23), it can be observed that only the heat fluxes across the boundary are considered in FVM, while only the temperature gradients within the control body are considered in FEM. These formulations, despite contradictory, may lead to an almost similar solution. Such a fact is due to the difference in the configuration of nodal-element integration. The configuration can be visualised in Figure 14.

In FEM, the integration boundary is located at the line/surface, which links the nodes, while in FVM, the integration boundary is located at the line/surface, which separates the nodes. In FVM, the heat flux can be applied to define the relations between the nodes because the heat flux vector is

positioned precisely in the adjacent nodes. Meanwhile, it is impractical, too, if we try to estimate the temperature distribution within the control volume because the corner of the control volume is not pinned with a node to store any variables' value. On the contrary, for FEM, there is no node located in adjacent heat flux of similar direction, and thus it is impractical too to estimate any temperature via heat flux across the integration boundary. To compensate for this shortcoming, FEM applies an interpolation function to predict the temperature distribution within the integration boundary; as we can see, the nodes are located at the corner of its integration boundary.

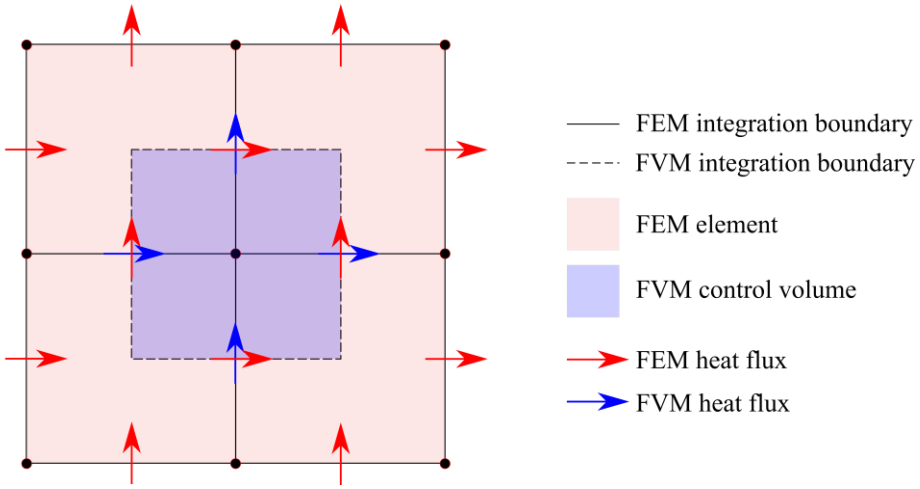

Fig. 14. Nodal-element configuration for FEM and FVM

Let us observe the central node in Figure 14 and prescribe the relations between the nodes via FEM and FVM. Apparently, the relations between the central node and its nodes can be formed using one integration domain when FVM is applied. However, we need four integration domains to form similar relations if FEM is applied. Moreover, FVM only interpolates four adjacent nodes to compute the value of a variable at the central node, while FEM interpolates eight adjacent nodes. The interpolation values formed via FEM and FVM can be illustrated in Figure 15. The nodal interpolation function for FVM can be shown in Eq. (24). If we re-write the nodal interpolation function for FEM in a way similar to FVM, Eq. (25) can be formed. The additional four nodal points required in FEM also implies that the formation of stiffness matrix and boundary conditions of FEM would be more complicated than FVM. Such a relatively complicated matrix would slow down the execution time, i.e., the time required for computer to generate the stiffness matrix and inverse the matrix.

$$T_{i,j} = -\frac{1}{4}\left(T_{i+1,j} + T_{i-1,j} + T_{i,j+1} + T_{i,j-1}\right) \tag{24}$$

$$T_{i,j} = -\frac{1}{8}\left(T_{i+1,j} + T_{i-1,j}\right) - \frac{1}{4}\left(T_{i,j+1} + T_{i,j-1}\right) - \frac{1}{16}\left(T_{i+1,j+1} + T_{i+1,j-1} + T_{i-1,j+1} + T_{i-1,j-1}\right) \tag{25}$$

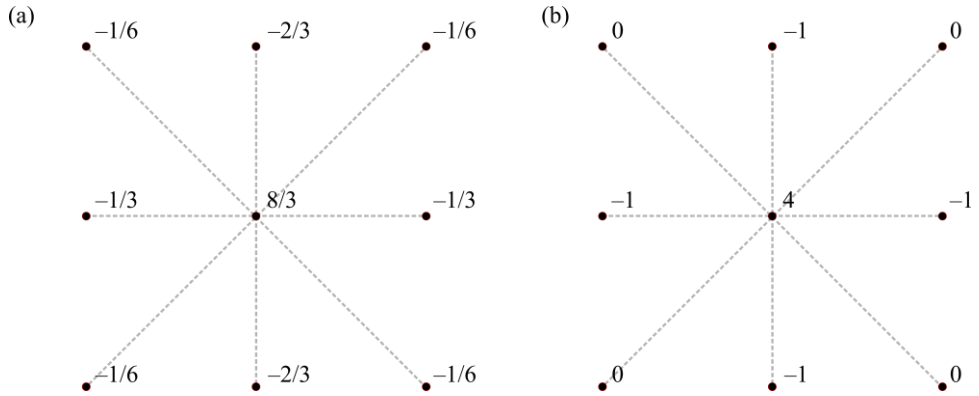

Fig. 15. Relations of interpolation constants for (a) GFEM and (b) FVM

According to the Leibniz theorem on fluid flow (see Eq. 26), the rate of change of an unsteady vector ϕ is equivalent to the net generation of ϕ within the control volume and the net flux of ϕ across the control surface [38].

$$\frac{d}{dt}\int_{V(t)} \phi \, dV = \int_{V(t)} \frac{d\phi}{dt} dV + \int_{A(t)} \phi\left(\vec{v}\cdot\vec{n}\right) \, dA \tag{26}$$

Make note that $\vec{n}$ signifies that the inflow and outflow of ϕ are directed orthogonally to the control surface. In other words, only the *x*- and *y*- direction adjacent nodes of the central node will be involved in the computation in a two-dimensional context. With this regard, the residuals of interpolation constants for FVM will be 0, which implies that FVM would ensure the conservativeness of the transport equation. Whereas in FEM, the residuals of the constants would be 2/3 if only the *x*- and *y*- adjacent direction nodes are considered. Such a residual would lead to unwanted under-prediction or over-prediction of results. This residual is also an important reason why the numerical error remained un-addressed, although the mesh size for GFEM is increased exponentially. Moreover, since the formulation of FVM can directly answer the call of Leibniz's theorem on fluid flow, FVM appears to be more conservative than FEM.

Several research studies also further verified our findings. Sváček *et al.,* [39] applied both FEM and FVM for 3D turbulent flow, and they concluded that FEM requires extra algorithm for executing the boundary conditions. Moreover, the stabilising technique in FEM requires further validation. Molina-Aiz *et al.,*[40] simulated the natural ventilation in greenhouses via FEM (ANSYS®/FLOTRAN v. 11.0) and FVM (ANSYS®/FLUENT v 6.3), and they found that FEM would provide a slightly larger value of ventilation rate. Moreover, FEM requires twice of the computational time taken by FVM, and 10 times of memory storage as required by FVM. Lopes *et al.,*[41] also compared the computational performance between FEM and FVM commercial software by simulating the fluid-structure interaction of blood flow, and they concluded that with sufficient number of grid size, both FVM and FEM would give identical results. Nonetheless, FEM (COMSOL®) required 483 hours of simulation time and 73.3 GB of memory storage, compared with 220 hours and 26.6 GB of FVM (ANSYS®). However, Frisani and Hassan [42] presented an interesting comparison of FEM and FVM in Immersed Boundary Method environment for flow across a stationary and moving cylinder at low Re. In IBM, FEM would provide a solution with superior accuracy compared with FVM, yet with the expense of extremely high computational effort.

Efforts are constantly made by various researchers to leverage the advantages of FEM and FVM for simulation by introducing hybrid FEM-FVM simulation techniques. Often, such FEM-FVM methods

were applied in fluid-structure Multiphysics problems. For instance, Sargado *et al.,*[43] and Asadi *et al.,*[44] proposed such strategy to simulate phase-field fracture and hydro-mechanical interactions in porous media, respectively. Moreover, it is a good idea to integrate the consideration of heat flux of FVM into FEM, whereby the spurious heat flux in this paper can be regarded as the residuals to be corrected by modifying the interpolation functions. Such refinement strategy can be done by incorporating the Residual Distribution method or Fluctuating Splitting method into FEM, and the mathematical discussion on the technique can be found in the work of van der Waide [45], Rossiello *et al.,*[46], Abgrall *et al.,*[47], Neoh and Ismail [48], and Colombo and Re [49]. There are more room of improvement for modifying FEM to be more conservative.

4. Conclusion

Despite the advantages and potentials explained in the Introduction, GFEM is prone to spurious heat flux and is not conservative compared with FVM in the two-dimensional domain. Over-prediction of temperature field between 2% to 4% can be observed. Moreover, GFEM is computationally more expensive (34% higher than FVM) and complex and is not as straightforward as FVM. Nonetheless, the temperature distribution pattern interpolated via GFEM is similar to the results obtained via FVM. More efforts need to be made to increase the accuracy and applicability of GFEM in CFD, such as improving the interpolation function and incorporating Residual Distribution method or Fluctuating splitting method into GFEM.

Acknowledgement

This research was funded by a grant from Ministry of Higher Education of Malaysia (FRGS Grant R.J130000.7824.4X172).

References

[1] Hutton, D. V. Basic Concept of the Finite Element Method, *Fundamentals in Finite Element Analysis*, 2004, 1–19.

[2] Mahur, B. P., Bhardwaj, Y. and Bansal, V. "Review on finite element analysis for estimation of residual stresses in welded structures." *Materials Today: Proceedings* 4, no. 9 (2017): 10230–10234. https://doi.org/10.1016/j.matpr.2017.06.354.

[3] Shetty, N., Shahabaz, S. M. and Sharma, S. S. "Divakara Shetty, S. A review on finite element method for machining of composite materials." *Composite Structures* 176 (2017): 790–802. https://doi.org/10.1016/j.compstruct.2017.06.012.

[4] Zhang, Z., Yu, J., Liu, H. and Chen, Z. "Experimental and finite element study on lateral global buckling of pipe-in-pipe structure by active control method." *Applied Ocean Research* 92 (2019): 101917. https://doi.org/10.1016/j.apor.2019.101917.

[5] Long, C. S., Loveday, P. W., Ramatlo, D. A. and Andhavarapu, E. V. "Numerical verification of an efficient coupled SAFE-3D FE analysis for guided wave ultrasound excitation." *Finite Elements in Analysis and Design* 149 (2018): 45–56. https://doi.org/10.1016/j.finel.2018.05.001.

[6] Yin, J., Xu, L., Wang, H., Xie, P., Huang, S., Liu, H., Yang, Z. and Li, B. "Accurate and fast three-dimensional free vibration analysis of large complex structures using the finite element method." *Computers & Structures* 221 (2019): 142–156. https://doi.org/10.1016/j.compstruc.2019.06.002.

[7] Cooper, R. J., Wilcox, R. K., Jones, A. C. "Finite element models of the tibiofemoral joint: A review of validation approaches and modelling challenges." *Medical Engineering & Physics* 74 (2019): 1–12. https://doi.org/10.1016/j.medengphy.2019.08.002.

[8] Hew, Z. C., Chan, B. T., Wan Ab Naim, W. N., Dokos, S., Tey, W. Y. and Liew, Y. M. Electro-Mechanical Finite Element Model of Left Ventricular Hypertrophy. In: Usman, J., Liew, Y.M., Ahmad, M.Y., Ibrahim, F. (eds) 6th Kuala Lumpur International Conference on Biomedical Engineering 2021. BIOMED 2021. IFMBE Proceedings, 86, 2022. Springer, Cham. https://doi.org/10.1007/978-3-030-90724-2_12.

[9] Mozafari, F., Thamburaja, P., Srinivasa, A. and Abdullah, S. "Fatigue life prediction under variable amplitude loading using a microplasticity-based constitutive model." *International Journal of Fatigue* 134 (2020): 105477. https://doi.org/10.1016/j.ijfatigue.2020.105477.

[10] Mozafari, F., Thamburaja, P., Moslemi, N. and Srinivasa, A. "Finite-element simulation of multi-axial fatigue loading in metals based on a novel experimentally-validated microplastic hysteresis-tracking method." *Finite Elements in Analysis and Design* 187 (2021): 103481. https://doi.org/10.1016/j.finel.2020.103481.

[11] Versteeg, H. K., Malalasekera, W. *An Introduction to Computational Fluid Dynamics: The Finite Volume Method* (Second.), 2004, Pearson Prentice Hall.

[12] Patankar, S. V. *Numerical Heat Transfer and Fluid Flow*, 1980.

[13] Lee, C. E., Tey, W. Y. and Tan, L. K. "The investigation on SIMPLE and SIMPLER algorithm through lid driven cavity." *Journal of Advanced Research in Fluid Mechanics and Thermal Sciences* 29 (2017): 10–23.

[14] Tey, W. Y., Wong, R., Asako, Y., Kang, H. S. and Ng, K. C. "Analysis on computational efficiency of convection discretisation schemes in SIMPLE algorithm." *Journal of Advanced Research in Fluid Mechanics and Thermal Sciences* 58, no. 1 (2019): 100–117.

[15] Peskin, C. S. "Numerical analysis of blood flow in the heart." *Journal of Computational Physics* 25, no. 3 (1977): 220–252. https://doi.org/10.1016/0021-9991(77)90100-0.

[16] Schwarz, S., Kempe, T. and Fröhlich, J. "An immersed boundary method for the simulation of bubbles with varying shape." *Journal of Computational Physics* 315 (2016): 124–149. https://doi.org/10.1016/j.jcp.2016.01.033.

[17] Mizuno, Y., Takahashi, S., Fukuda, K. and Obayashi, S. "Direct numerical simulation of gas-particle flows with particle-wall collisions using the immersed boundary method." *Applied Sciences* 8, no. 12 (2018): 2387. https://doi.org/10.3390/app8122387.

[18] Belytschko, T., Lu, Y. Y. and Gu, L. "Element-free Galerkin methods." *International Journal for Numerical Methods in Engineering* 37, no. 2 (1994): 229–256. https://doi.org/10.1002/nme.1620370205.

[19] Belytschko, T., Lu, Y. Y. and Gu, L. "Crack propagation by element-free Galerkin methods." *Engineering Fracture Mechanics* 51, no. 2 (1995): 295–315. https://doi.org/10.1016/0013-7944(94)00153-9.

[20] Belytschko, T., Lu, Y. Y., Gu, L. and Tabbara, M. "Element-free galerkin methods for static and dynamic fracture." *International Journal of Solids and Structures* 32, nos. 17–18 (1995): 2547–2570. https://doi.org/10.1016/0020-7683(94)00282-2.

[21] Dolbow, J. and Belytschko, T. "An introduction to programming the meshless Element Free Galerkin method." *Archives of Computational Methods in Engineering*. *State of the Art Reviews* 5, no. 3 (1998): 207–241. https://doi.org/10.1007/bf02897874.

[22] Tey, W. Y., Asako, Y., Ng, K. C. and Lam, W.-H. "A review on development and applications of element-free galerkin methods in computational fluid dynamics." *International Journal for Computational Methods in Engineering Science and Mechanics* 21, no. 5 (2020): 252–275. https://doi.org/10.1080/15502287.2020.1821126.

[23] Wang, J. G. and Liu, G. R. "A point interpolation meshless method based on radial basis functions." *International Journal for Numerical Methods in Engineering* 54, no. 11 (2002): 1623–1648, 2002. https://doi.org/10.1002/nme.489.

[24] Atluri, S. N. and Zhu, T. "A new Meshless Local Petrov-Galerkin (MLPG) approach in computational mechanics." *Computational Mechanics* 22, no. 2 (1998): 117–127. https://doi.org/10.1007/s004660050346.

[25] Bathe, K.-J. and Baig, M. M. I. "On a composite implicit time integration procedure for nonlinear dynamics." *Computers & Structures* 83, nos. 31–32 (2005): 2513–2524. https://doi.org/10.1016/j.compstruc.2005.08.001.

[26] Vanselow, R. "Relations between FEM and FVM applied to the poisson equation." *Computing* 57, no. 2 (1996): 93–104. https://doi.org/10.1007/BF02276874.

[27] Ahmad, N., Rappaz, J., Desbiolles, J.-L., Jalanti, T., Rappaz, M., Combeau, H., Lesoult, G. and Stomp, C. "Numerical simulation of macrosegregation: A comparison between finite volume method and finite element method predictions and a confrontation with experiments." *Metallurgical and Materials Transactions A* 29, no. 2 (1998): 617–630. https://doi.org/10.1007/s11661-998-0143-9.

[28] Guoya Dong, Zou, J., Bayford, R. H., Xinshan Ma, Shankai Gao, Weili Yan and Manling Ge. "The comparison between FVM and FEM for EIT forward problem." *IEEE Transactions on Magnetics* 41, no. 5 (2005): 1468–1471. https://doi.org/10.1109/TMAG.2005.844558.

[29] Jeong, W. and Seong, J. "Comparison of effects on technical variances of computational fluid dynamics (CFD) software based on finite element and finite volume methods." *International Journal of Mechanical Sciences* 78 (2014): 19–26. https://doi.org/10.1016/j.ijmecsci.2013.10.017.

[30] Wang, B.-L. and Mai, Y.-W. "Transient one-dimensional heat conduction problems solved by finite element." *International Journal of Mechanical Sciences* 47, no. 2 (2005): 303–317. https://doi.org/10.1016/j.ijmecsci.2004.11.001.

[31] Dhawan, S. and Kumar, S. "Comparative study of numerical techniques for 2d transient heat conduction equation." *International Journal of Research and Reviews in Applied Sciences* 1, no. 1 (2009): 38–46.
[32] Peiró, J. and Sherwin, S. Finite Difference, Finite Element and Finite Volume Methods for Partial Differential Equations, *Handbook of Materials Modelling*, 2005, 2415–2446.
[33] Hutton, D. V. Applications in Heat Transfer, *Fundamentals of Finite Element Analysis*, 2004, McGraw Hill Companies, Inc.
[34] Versteeg, H. K., Malalasekara, W. The Finite Volume Method for Diffusion Problems, *An Introduction to Computational Fluid Dynamics: The Finite Volume Method* (Second.), 2007, Pearson Prentice Hall, 115–134
[35] Kajishima, T., Taira, K. *Computational Fluid Dynamics: Incompressible Turbulent Flows*, 2018, Springer
[36] Demirdzic, I. Finite volumes vs finite elements. There is a choice, *Coupled Systems Mechanics*, vol. 9, 5–28, 2020.
[37] Wu, C.-C., Völker, D., Weisbrich, S. and Neitzel, F. "The finite volume method in the context of the finite element method." *Materials Today: Proceedings* 62 (2022): 2679–2683. https://doi.org/10.1016/j.matpr.2022.05.460.
[38] Cengel, Y. A., Cimbala, J. M. Chapter 4: Fluid Kinematics, *Fluid Mechanics: Fundamentals and Applications*, 2014, McGraw-Hill Inc., 133–184.
[39] Sváček, P., Louda, P. and Kozel, K. "On numerical simulation of three-dimensional flow problems by finite element and finite volume techniques." *Journal of Computational and Applied Mathematics* 270 (2014): 451–461. https://doi.org/10.1016/j.cam.2013.12.019.
[40] Molina-Aiz, F. D., Fatnassi, H., Boulard, T., Roy, J. C. and Valera, D. L. "Comparison of finite element and finite volume methods for simulation of natural ventilation in greenhouses." *Computers and Electronics in Agriculture* 72, no. 2 (2010): 69–86. https://doi.org/10.1016/j.compag.2010.03.002.
[41] Lopes, D., Agujetas, R., Puga, H., Teixeira, J., Lima, R., Alejo, J. P. and Ferrera, C. "Analysis of finite element and finite volume methods for fluid-structure interaction simulation of blood flow in a real stenosed artery." *International Journal of Mechanical Sciences* 207 (2021): 106650. https://doi.org/10.1016/j.ijmecsci.2021.106650.
[42] Frisani, A. and Hassan, Y. A. "On the immersed boundary method: Finite element versus finite volume approach." *Computers & Fluids* 121 (2015): 51–67. https://doi.org/10.1016/j.compfluid.2015.08.006.
[43] Sargado, J. M., Keilegavlen, E., Berre, I. and Nordbotten, J. M. "A combined finite element–finite volume framework for phase-field fracture.", *Computer Methods in Applied Mechanics and Engineering* 373 (2021): 113474. https://doi.org/10.1016/j.cma.2020.113474.
[44] Asadi, R. and Ataie-Ashtiani, B. "Hybrid finite volume-finite element methods for hydro-mechanical analysis in highly heterogeneous porous media." *Computers and Geotechnics* 132 (2021): 103996. https://doi.org/10.1016/j.compgeo.2020.103996.
[45] van der Weide. *Compressible Flow Simulation on Unstructured Grids using Multi-dimensional Upwind Schemes*, 1998 Delft University.
[46] Rossiello, G., de Palma, P., Pascazio, G. and Napolitano, M. "Second-order-accurate explicit fluctuation splitting schemes for unsteady problems." *Computers & Fluids* 38, no. 7 (2009): 1384–1393. https://doi.org/10.1016/j.compfluid.2008.01.021.
[47] Abgrall, R., Bacigaluppi, P. and Tokareva, S. "High-order residual distribution scheme for the time-dependent Euler equations of fluid dynamics." *Computers & Mathematics with Applications* 78, no. 2 (2019): 274–297. https://doi.org/10.1016/j.camwa.2018.05.009.
[48] Neoh, S. S. and Ismail, F. "Residual distribution schemes for Maxwell's equations." *Applied Mathematics and Computation* 348 (2019): 275–317. https://doi.org/10.1016/j.amc.2018.11.055.
[49] Colombo, S. and Re, B. "An ALE residual distribution scheme for the unsteady Euler equations over triangular grids with local mesh adaptation." *Computers & Fluids* 239 (2022): 105414. https://doi.org/10.1016/j.compfluid.2022.105414.